OPEN

Oncogene (2016) 35, 691–701

www.nature.com/onc

ORIGINAL ARTICLE

Functional proteomics identifies miRNAs to target a p27/Myc/phospho-Rb signature in breast and ovarian cancer

This article has been corrected since Advance Online Publication and a corrigendum is also printed in this issue

EG Seviour[1,11], V Sehgal[1,11], Y Lu[1,11], Z Luo[1,11], T Moss[1], F Zhang[1], SM Hill[2], W Liu[3], SN Maiti[4], L Cooper[4], R Azencot[5], G Lopez-Berestein[6,7], C Rodriguez-Aguayo[6], R Roopaimoole[6], CV Pecot[8], AK Sood[9], S Mukherjee[2], JW Gray[10], GB Mills[1,11] and PT Ram[1,11]

The myc oncogene is overexpressed in almost half of all breast and ovarian cancers, but attempts at therapeutic interventions against myc have proven to be challenging. Myc regulates multiple biological processes, including the cell cycle, and as such is associated with cell proliferation and tumor progression. We identified a protein signature of high myc, low p27 and high phospho-Rb significantly correlated with poor patient survival in breast and ovarian cancers. Screening of a miRNA library by functional proteomics in multiple cell lines and integration of data from patient tumors revealed a panel of five microRNAs (miRNAs) (miR-124, miR-365, miR-34b*, miR-18a and miR-506) as potential tumor suppressors capable of reversing the p27/myc/phospho-Rb protein signature. Mechanistic studies revealed an RNA-activation function of miR-124 resulting in direct induction of p27 protein levels by binding to and inducing transcription on the p27 promoter region leading to a subsequent G1 arrest. Additionally, *in vivo* studies utilizing a xenograft model demonstrated that nanoparticle-mediated delivery of miR-124 could reduce tumor growth and sensitize cells to etoposide, suggesting a clinical application of miRNAs as therapeutics to target the functional effect of myc on tumor growth.

Oncogene (2016) **35,** 691–701; doi:10.1038/onc.2014.469; published online 2 February 2015

INTRODUCTION

The expression and activity of myc transcription factor is frequently deregulated in cancer and efforts to target it have been challenging.[1] Myc has an important regulatory role in multiple pathways, including cell cycle,[2,3] metabolism[4,5] and cellular architecture;[6,7] however, its role in the cell cycle is directly related to the proliferative capacity of cancer cells. The cell proliferative effect of myc can be coupled to changes in levels and activity of the cyclin-dependent kinase inhibitor p27/kip, whereby myc activity can lead to decreased levels of p27.[8,9] Decreased levels of p27 are tightly associated with increased phosphorylation of the retinoblastoma protein Rb.[10,11] Therefore, a high myc, low p27 and high phospho-Rb signature is indicative of increased cell cycle progression and proliferation. We investigated whether such a signature of high myc, low p27 and high phospho-Rb protein levels measured from breast and ovarian cancer patients had a significant correlation with patient survival. Further, we wanted to determine whether novel therapeutic strategies using microRNAs (miRNAs) could be utilized to counter the myc/p27/phospho-Rb cell proliferative signature.

miRNAs are small RNA molecules, approximately 22 nucleotides in length, which have critical roles in the maintenance of cellular homeostasis.[12,13] Although the ability of miRNAs to regulate mRNA levels is well established,[14–16] their role in the regulation of intracellular signaling events is less well defined. We therefore sought to use a functional proteomic screening approach, combined with the integration of patient data from The Cancer Genome Atlas (TCGA) database, to identify clinically relevant miRNAs able to reverse a myc/p27/phospho-Rb signature. As miRNAs are predicted to target numerous genes, we additionally sought to integrate phenotypic observations with predicted and validated targets of the identified miRNA to determine the functional consequences of their perturbations. With recent clinical trials utilizing non-coding RNA for therapeutics we wanted to ascertain whether appropriate chemotherapy can be used in combination with the miRNAs to enhance cancer cell death and tumor ablation in mouse models.

Here we identified the cell cycle protein expression signature of myc, p27 and phospho-Rb in breast and ovarian cancer patients that significantly correlates with patient survival. Using this signature, we performed an miRNA screen coupled to reverse-phase protein array to identify candidate miRNA that could functionally reverse this protein and phospho-protein signature and identified a set of 56 candidate miRNAs that could both reverse the protein signature as well as reduce cell proliferation. From these candidates, we performed an additional screen in two other cell lines and integrated data from patient tumor samples to identify a candidate miRNA, miR-124, which reduced myc and phospho-Rb while increasing p27 protein levels across multiple cell lines. Detailed analysis of miR-124 showed that the

[1]Department of Systems Biology, UT MD Anderson Cancer Center, Houston, TX, USA; [2]MRC Biostatistics Unit, Cambridge Institute of Public Health, Cambridge, UK; [3]Department of Bioinformatics and Computational Biology, UTMDACC, Houston, TX, USA; [4]Department of Pediatrics, UTMDACC, Houston, TX, USA; [5]Department of Mathematics, University of Houston, Houston, TX, USA; [6]Department of Experimental Therapeutics, UTMDACC, Houston, TX, USA; [7]Center for RNA Interference and Non-Coding RNA, UTMDACC, Houston, TX, USA; [8]Division of Cancer Medicine, UTMDACC, Houston, TX, USA; [9]Department of Gynecologic Oncology, UTMDACC, Houston, TX, USA and [10]Department of Biomedical Engineering, Oregon Health Sciences University, Portland, OR, USA. Correspondence: Dr P Ram, Department of Systems Biology, University of Texas MD Anderson Cancer Center, 1515 Holcombe Boulevard, Houston, TX 77030, USA.
E-mail: pram@mdanderson.org
[11]These authors contributed equally to this work.
Received 19 June 2014; revised 16 December 2014; accepted 19 December 2014; published online 2 February 2015

mechanism of reversal of the myc/p27/phospho-Rb signature was by an RNA activation function of miR-124. Although activating functions of miRNAs have been shown to be possible using synthetic gene constructs, here we use proteomic analysis to identify activation of an endogenous gene by miRNAs, whereby the expression of miR-124 increased p27 protein levels. This led to a subsequent G1 arrest, thereby leading to a loss of phospho-Rb and decrease in myc protein levels. Further, we demonstrate that miR-124 can block cell invasion and proliferation. Clinical implications of miR-124 as a possible therapeutic agent in late-stage breast and ovarian cancers was explored with its use in combination with etoposide, a chemotherapy commonly used in such patients. Etoposide sensitivity and resistance is associated with increased integrin β1 levels in patients,[17–20] which makes miR-124 a highly relevant therapeutic agent as miR-124 can also directly target and reduce integrin β1. Therefore we demonstrate here a highly clinically relevant miRNA that can both reverse the myc/p27/phospho-Rb protein signature to target cell proliferation while at the same time block integrin β1 and increase sensitivity to etoposide in breast and ovarian cancers.

RESULTS

Identification of a myc/p27/phospho-RB signature associated with survival

We analyzed reverse-phase protein array (RPPA) data (obtained from the TCGA data portal) from breast and ovarian cancer patients to identify a signature comprised of low p27, high myc and high phospho-Rb protein levels in breast and ovarian tumors (Figure 1a). Clinical outcome analysis of patients with this protein signature showed a significant correlation of the signature with poor survival in both breast and ovarian cancer patients (Figure 1b). Efforts to target myc with pharmacological compounds have proved to be challenging, and therefore we utilized a functional approach to identify potential miRNAs as therapeutics that could target the cell cycle myc/p27/phospho-Rb protein signature. In order to identify miRNAs capable of reversing this signature, we expressed a library of 879 miRNAs in MDA-MB-231 (triple negative) breast cancer cell line and analyzed the protein levels of myc, phospho-Rb and p27 by RPPA, as well as measuring changes in the cell number induced by each miRNA (Supplementary Figure S1). Analysis determined that 56 miRNAs reversed the expression of all three proteins in the signature in addition to reducing cellular proliferation (Figure 1c). A subset of this group of miRNAs, along with others selected from the other groups (Supplementary Figure S2), were rescreened in MDA-MB-231 cells in addition to two ovarian cancer cell lines HeyA8 and SKOV3.ip1. miRNAs were selected for the secondary screen based on multiple criteria, including downregulation of previously validated targets and regulation of previously unvalidated targets of interest. Comparison of the two independent screens in MDA-MB-231 cells revealed 70% true positives between the two screens. From the miRNA-RPPA analysis across the different cell types, we determined that only one miRNA reversed the expression of all three proteins in all three cell lines, miR-18a. As this is a known oncomiR associated with tumor progression and poor clinical outcome in multiple cancer types,[21–24] and so would not be suitable as a potential therapeutic intervention, we chose to consider miRNAs that reversed at least two of the three signature proteins. We identified an additional four candidate miRNAs (miR-124, miR-365, miR-34b* and miR-506) that reversed the expression of at least two of the three proteins in the signature in all three of the cell lines (Figure 1d). miRNA levels in all three cell lines were measured using the Nanostring nCounter miRNA expression assay, and the data showed that miR-124 was the lowest expressed of the five in two cell lines and the second lowest of the five in the third cell line (Supplementary Figure S3). Copy number analysis of TCGA breast and ovarian cancer data showed that all five miRNAs had significant heterozygous loss in ovarian cancers and four of the five had loss in breast cancer. Of these candidate miRNAs, the data showed that miR-124, located on the 8p23.1 chromosome region, was the most commonly lost miRNA in patients from both cancer types (Figure 1e), indicating a potential role for this miRNA as a tumor suppressor. Analysis of the data from additional cancer types confirmed the loss of the miR-124 chromosomal region across multiple cancer types (Supplementary Figure S4), suggesting that this miRNA is of high clinical significance in cancer patients. Additionally, 44% of genes shown to confer synthetic lethality of myc-overexpressing tumors[25] were predicted to be targets of miR-124, suggesting that miR-124 could function as a potent tumor suppressor in cancers with high myc expression (Supplementary Figure S5).

miR-124 regulates p27 *in vitro*

We performed western blotting analysis in a panel of cell lines spanning multiple tumor types to confirm the ability of miR-124 to reverse the p27 low/myc high/phospho-Rb high signature and found that indeed miR-124 expression leads to an increase in p27 and a concurrent decrease in myc and phospho-Rb protein levels (Figure 2a). As neither the 3′ untranslated region of myc nor Rb contain predicted target sites for miR-124, and the increase in p27 was consistent across all the cell lines studied, with more variation in the response of myc and phospho-Rb to miR-124 expression, we hypothesized that miR-124 may regulate these proteins through inducing p27 expression and subsequent cell cycle arrest. In order to determine whether the miR-124-induced increase in p27 was due to *de novo* protein synthesis or increased stability of existing protein, we treated the cells with cycloheximide. The data show that the increase in p27 is due to *de novo* protein synthesis whereby cycloheximide blocks the increase in p27 levels upon expression of miR-124 (Figure 2b). Previous studies have suggested that miRNA binding to promoter regions can induce gene expression.[26–29] To determine whether miR-124 can induce p27 expression directly, we analyzed the p27 promoter region, which indicated a potential binding site for miR-124 (Figure 2c). We cloned the p27 promoter region upstream of the luciferase gene and performed a luciferase assay and observed that indeed miR-124 can directly increase luciferase activity downstream of the p27 promoter region (Figure 2d). To determine whether the increase in luciferase activity mediated by miR-124 was a result of its binding to the p27 promoter region, we mutated the miR-124-binding site within the p27 promoter region, which prevented the miR-124-induced activity, suggesting that miR-124 binding to the p27 promoter region causes the induction of p27 expression by miR-124. Induction of p27 was also abrogated by transfection of the antisense inhibitor of miR-124 which had no effect on luciferase expression from either the wild-type or mutated p27 promoter (Figure 2d).

To determine whether the increase in p27 and decrease in myc and phospho-Rb protein levels stimulated by miR-124 induced changes in cell cycle progression, we analyzed miR-124-transfected cells and observed a significant increase in the G1 phase population, with a concurrent decrease in the S phase population consistent with expression patterns of p27, myc and phospho-Rb proteins (Figure 2e). In order to demonstrate that the change in cell cycle induced by miR-124 was dependent on the expression of p27, we transfected siRNA targeting p27, and the data show that the miR-124-induced alterations in the cell cycle distribution are lost upon targeting p27 with siRNA (Figure 2f). To determine whether the miR-124-mediated decrease in myc and phospho-Rb are dependent on induction of p27, we co-transfected p27 siRNA and found that the miR-124-mediated decrease in myc and phospho-Rb are, at least partially, dependent on p27, confirming that the reversal of the signature by miR-124 is

primarily dependent on the ability of miR-124 to induce p27 (Figure 2g), although other, as yet unidentified, miR-124 targets may also be involved in this process.

miR-124 functions as a tumor suppressor

Having observed the p27 induction and myc and phospho-Rb decrease by miR-124 as well as a decrease in cell cycle progression, we

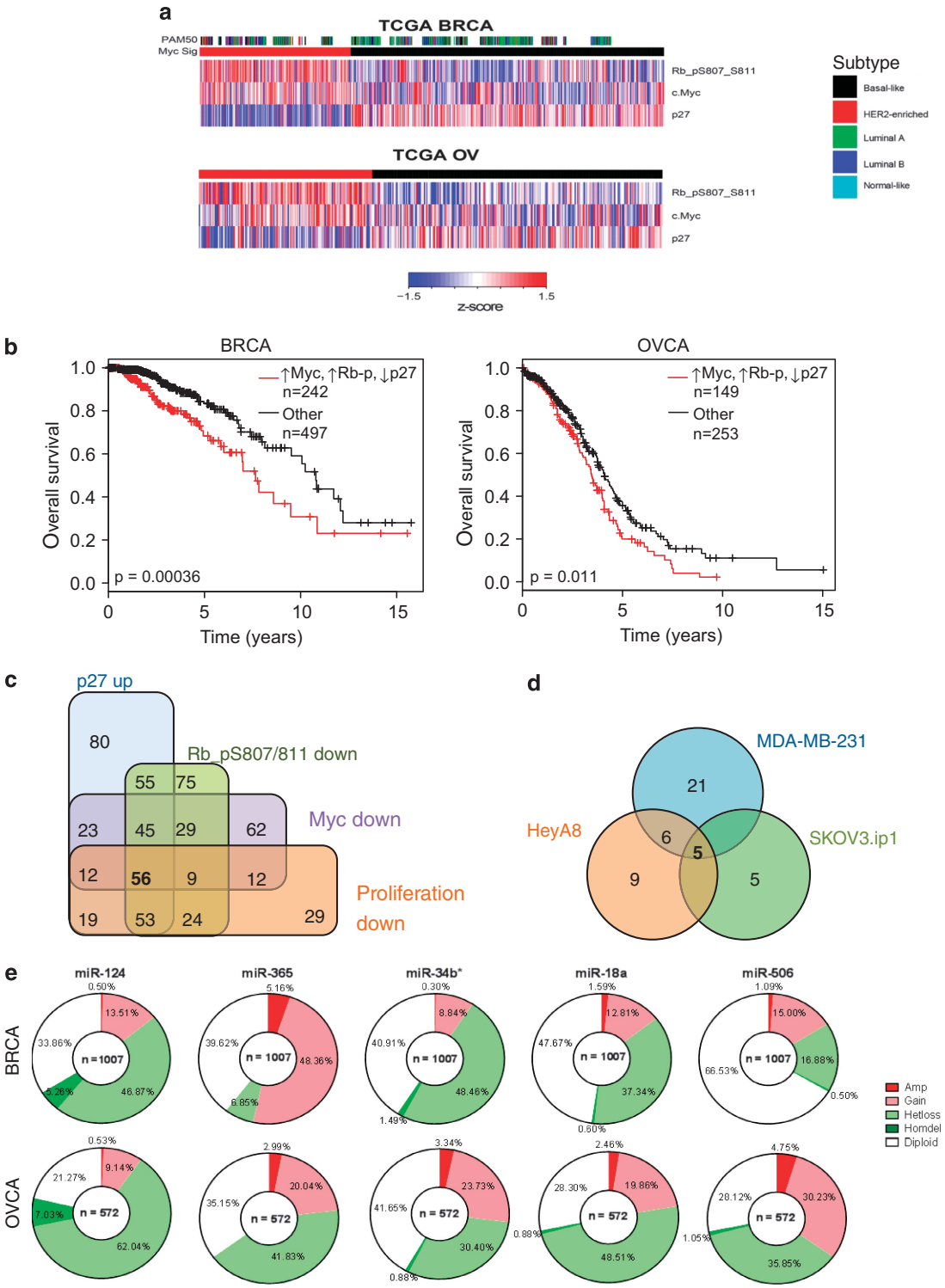

Figure 1. Identification of miR-124 as a clinically significant miRNA. (**a**) Hierarchical clustering of TCGA RPPA data identifies a subset of breast (BRCA) and ovarian (OVCA) cancer patients exhibiting a myc high, phospho-Rb high, p27 low protein signature (red). Where available, PAM50 subtype is included for BRCA samples. (**b**) Expression of the myc/phospho-Rb/p27 signature is associated with poor survival in breast and ovarian cancer patients. (**c**) miRNAs that reversed the signature in a screen of 879 miRNAs in MDA-MB-231 cells coupled to decreased proliferation, a subset of which were selected for further investigation. (**d**) miRNAs that were able to reverse at least two of the three components of the signature in each of the cell lines in the secondary screen. (**e**) Copy number analysis of the five miRNAs able to reverse the signature in all three cell lines in breast and ovarian cancer patients.

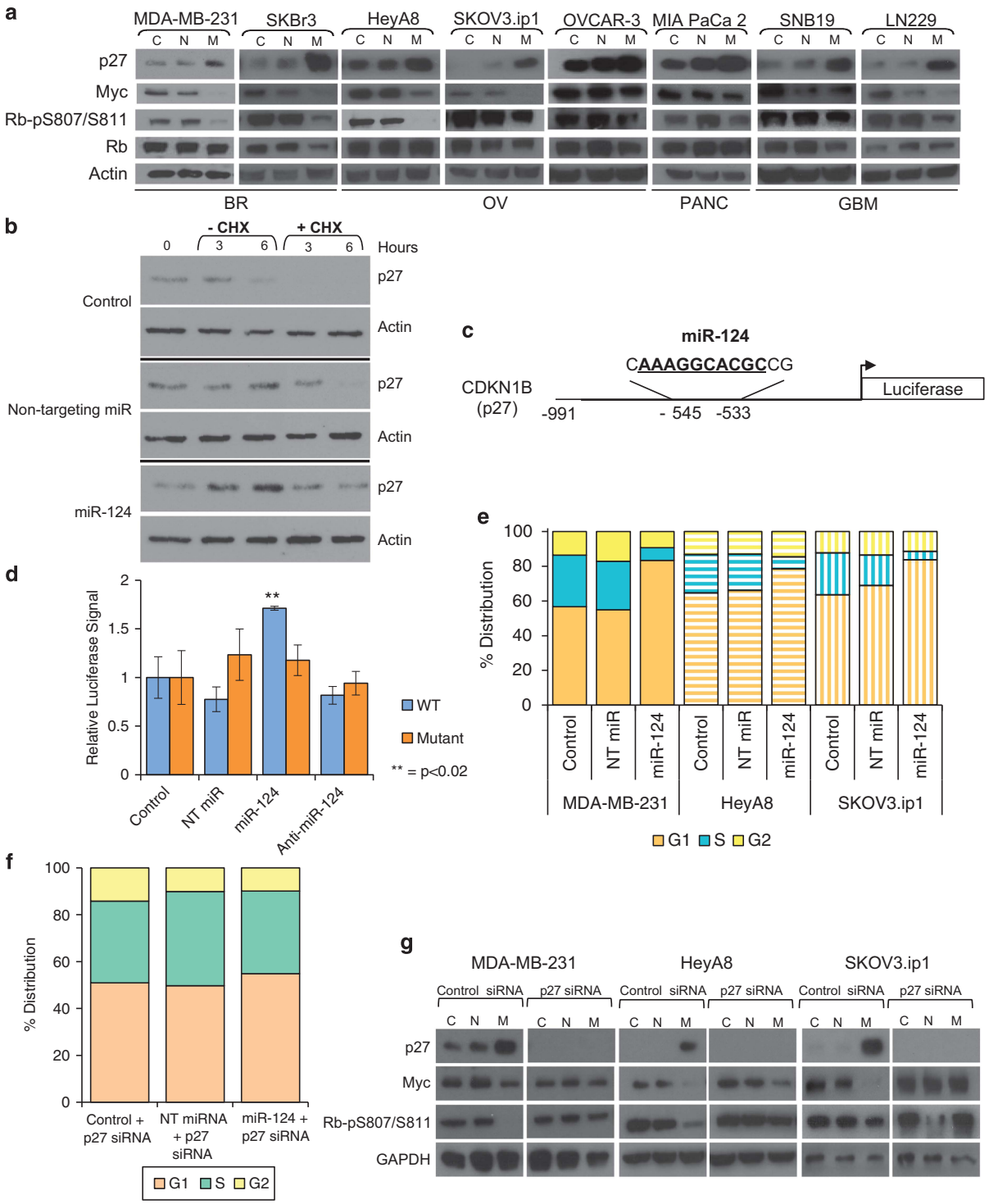

Figure 2. miR-124 regulates p27. (**a**) A panel of cell lines from varying tumor types, including breast (BR), ovarian (OV), pancreatic (PANC) and glioblastoma multiforme (GBM), were transfected with either non-targeting miRNAs (N) or miR-124 (M) or treated with transfection reagent alone (C) for 48 h. Expression of the myc/p27/phospho-Rb signature was analyzed by western blotting. (**b**) Protein levels were analyzed by western blotting at the indicated time points after miRNA transfection and cycloheximide treatment. (**c**) Potential miR-124-binding site in the p27 promoter. (**d**) Expression of luciferase downstream of the wild-type p27 promoter (WT) or the p27 promoter following mutation of the miR-124-binding site (Mutant). (**e**) miR-124 induces G1 arrest. Cell cycle distribution was determined in MDA-MB-231 (solid bars), HeyA8 (horizontal stripes) and SKOV3.ip1 (vertical stripes) cells by flow cytometry following staining with propidium iodide. Orange bars indicate the percentage of cells in G1 phase, blue bars represent S phase and yellow bars indicate G2 phase. (**f**) miR-124-induced cell cycle alterations require p27. HeyA8 cells were transfected with the indicated miRNAs in combination with siRNA targeting p27 for 48 h. Cells were fixed and stained with propidium iodide, and cell cycle phase was determined by flow cytometry. (**g**) miR-124 regulates myc and phospho-Rb through p27. MDA-MB-231, HeyA8 and SKOV3.ip1 cells were transfected with the indicated miRNAs in combination with siRNA targeting p27 for 48 h. Expression of p27, myc and phospho-Rb were analyzed by western blotting.

wanted to determine the functional phenotypic changes of miR-124 expression. Consistent with a tumor-suppressor function, miR-124 significantly reduced cellular proliferation (Figure 3a). Further, miR-124 also significantly reduced migration in a wound-healing assay (Figure 3b) as well as invasion through Matrigel-coated chambers (Figure 3c). These data suggested that miR-124 could function as a potent tumor suppressor by reversing the p27/myc/phospho-Rb protein survival signature, inducing cell cycle arrest and inhibiting proliferation, migration and invasion.

We additionally observed that miR-124-transfected cells exhibited morphological changes associated with reorganization of the actin cytoskeleton (Figure 3d). AGO-CLIP-seq analyses of miR-124 targets showed a large interconnected network of genes that included the integrin β1 network. Consistent with these findings and previous studies showing that miR-124 can directly target the 3′ untranslated region of integrin β1,[30,31] western blotting analysis revealed a decrease in the expression of integrin β1 in a panel of cell lines spanning multiple tumor types (Figure 3e). Concordantly, the miR-124-induced loss of integrin β1 expression significantly reduced adherence to a panel of extracellular matrices, including collagen I, laminin, fibronectin and vitronectin, as well as to uncoated plates (Figure 3f), suggesting that the miR-124-mediated decrease in integrin β1 levels was of functional consequence. Since miRNAs, including miR-124, are known to target multiple genes and proteins, analysis of the effect of miR-124 on cellular proliferation revealed a functional role for both p27 and integrin β1 in miR-124-mediated reduction of proliferation in certain contexts. The data showed that neither overexpression of p27 nor knockdown of integrin β1 alone was sufficient to recapitulate the effect of miR-124, while the combination of both most closely resembled the effect of miR-124 on proliferation in HeyA8 cells. However, overexpression of p27 was sufficient to mimic miR-124 overexpression in both MDA-MB-231 and SKOV3.ip1 cells, suggesting that the specific miR-124 targets involved in the regulation of proliferation may be dependent on mutational background or other context-dependent factors (Figure 3g). Additionally, to determine the requirement for either p27 or integrin β1 in the effects of miR-124 on cellular motility, we expressed miR-124 in combination with either an siRNA targeting p27, a plasmid overexpressing integrin β1 or both and repeated the wound-healing assay. The data showed that while either the loss of p27 or the replacement of integrin β1 could partially negate the effects of miR-124 on cellular motility, the combination was able to reverse the miR-124-mediated inhibition of wound healing in all three cell lines (Supplementary Figure S6).

miR-124 sensitizes cells to etoposide

Having identified miR-124 as a potential tumor suppressor that could functionally target the p27/myc/phospho-Rb protein signature, we wanted to determine whether miR-124 could be utilized as a therapeutic agent in breast and ovarian cancers. Clinical applications of new modalities are tested in late-stage cancer patients, and given the previously identified role for integrin β1 in mediating etoposide resistance,[17–20] we hypothesized that the expression of miR-124 would sensitize cells to etoposide in tumor models. *In vitro* analysis of HeyA8 cells overexpressing miR-124 showed increased sensitivity to etoposide whereby miR-124-expressing cells exhibited a twofold greater sensitivity to etoposide ($IC_{50} = 42.19$ nM) as compared with control ($IC_{50} = 91.84$ nM) (Figure 4a). We measured apoptotic cell death, and the data showed that the combination of miR-124 and etoposide increased apoptosis (Figure 4b) relative to either treatment alone. To determine the potential use of miR-124 as a therapeutic agent in inhibiting tumor growth *in vivo*, we utilized 1,2-dioleoyl-sn-glycero-3-phosphocholine (DOPC)-nanoparticle delivery of miR-124 to tumors implanted in the peritoneal cavity of athymic nude mice. While previous *in vivo* studies of miR-124 have relied on expression of miR-124 by transfection[32] or viral transduction of tumor cells prior to inoculation of the mice[33–38] or on injection of miRNA directly into the tumor,[39] the use of DOPC-nanoparticles allows the study of the effects of miR-124 *in vivo* following intraperitoneal injection of the miRNA, thereby more closely replicating the conditions for treatment of human patients. Delivery of miR-124–DOPC alone significantly decreased tumor volume and the number of tumors formed in both MDA-MB-231 (Figure 4c) and SKOV3.ip1 (Figure 4d) models. Treatment of mice with etoposide alone also significantly decreased tumor volume and, excitingly, the combination of miR-124 and etoposide further decreased tumor volume and numbers (Figures 4c and d) compared with either treatment alone. Histological analysis of the tumors showed that, in the animals treated with miR-124, there was a decrease in integrin β1 and increase in p27 in the tumors demonstrating that miR-124 had the same functional activity as was observed *in vitro* (Figure 4e).

DISCUSSION

Targeting important oncogenes such as K-Ras and myc with drugs has been a tremendous challenge. Alternative strategies to target these hard-to-drug oncogenes include understanding the functional downstream networks that they regulate by identifying the signatures associated with their signaling. One of the more promising avenues to target hard-to-drug molecules has been the use of RNAi, owing to its ability to regulate key oncogenes regardless of inherent activating mutations.[40] Indeed a clinical trial of miRNA therapeutics is ongoing (http://clinicaltrials.gov/ct2/show/NCT01829971). One of the potential criticisms of the use of miRNAs has been the relatively large number of putative gene targets. However, one could use this 'shotgun' action of miRNAs as an advantage by identifying the functional changes induced by these miRNAs and then asking under what contexts these miR targets could be advantageous therapeutically. Therefore, rather than identifying one target, we utilized a systems approach of identifying a clinically significant myc network signature and then using the broad action of miRNAs to identify candidates that could reverse this signature. A protein signature rather than an mRNA or gene signature allows for a functional analysis of patient data, and recent analyses of TCGA data suggest that the knowledge gain is largest at the protein level.[41] Therefore, we utilized the proteomic p27, myc, phospho-Rb signature to identify miRNAs that may be useful as therapeutic modalities. As anticipated, the screen revealed a number of miRNAs that could reverse the signature even after expansion of the secondary screen to include three different cell lines. Rather than further expanding the screen to include additional cell lines, we utilized clinical data to determine whether the identified miRNAs were dysregulated in the patients' tumors. Starting with clinical data, performing a miRNA-proteomic screen in multiple cell lines and returning to patient data to filter the screen results is a powerful iterative process to identify clinically high-value targets. Being completely unbiased through this process identified miR-124 as the leading candidate, and the power of this method was validated by findings from other investigators who have demonstrated the clinical significance of miR-124 in other cancer types, such as oral, prostate, glioma, liver and endometrial cancers.[31,33,35,36,38,42–44]

One of the challenges in the use of non-coding RNA is the issue of delivery and toxicity. Recent work by Sood and colleagues has demonstrated the efficiency of using nanoparticles to deliver non-coding RNA, including siRNA and miRNA, to established xenograft tumors in mice.[45] These delivery agents are associated with low toxicity and immune responses and promise to be useful for delivery of non-coding RNA for therapeutics. Using this approach in combination with chemotherapy can be advantageous in increasing tumor cell killing and potentially also target factors that may induce adaptive resistance to the

chemotherapeutic agent. Here we show that the multi-gene targeting of miR-124 includes integrin β1, whose increased expression is associated with insensitivity to etoposide, which could be an advantage in combining miRNAs with chemotherapy. Indeed the addition of miR-124 increases sensitivity to etoposide resulting in increased cell death.

Significant loss of miR-124 in breast and ovarian cancer patients coupled to the multi-modal effect of miR-124 on inducing p27,

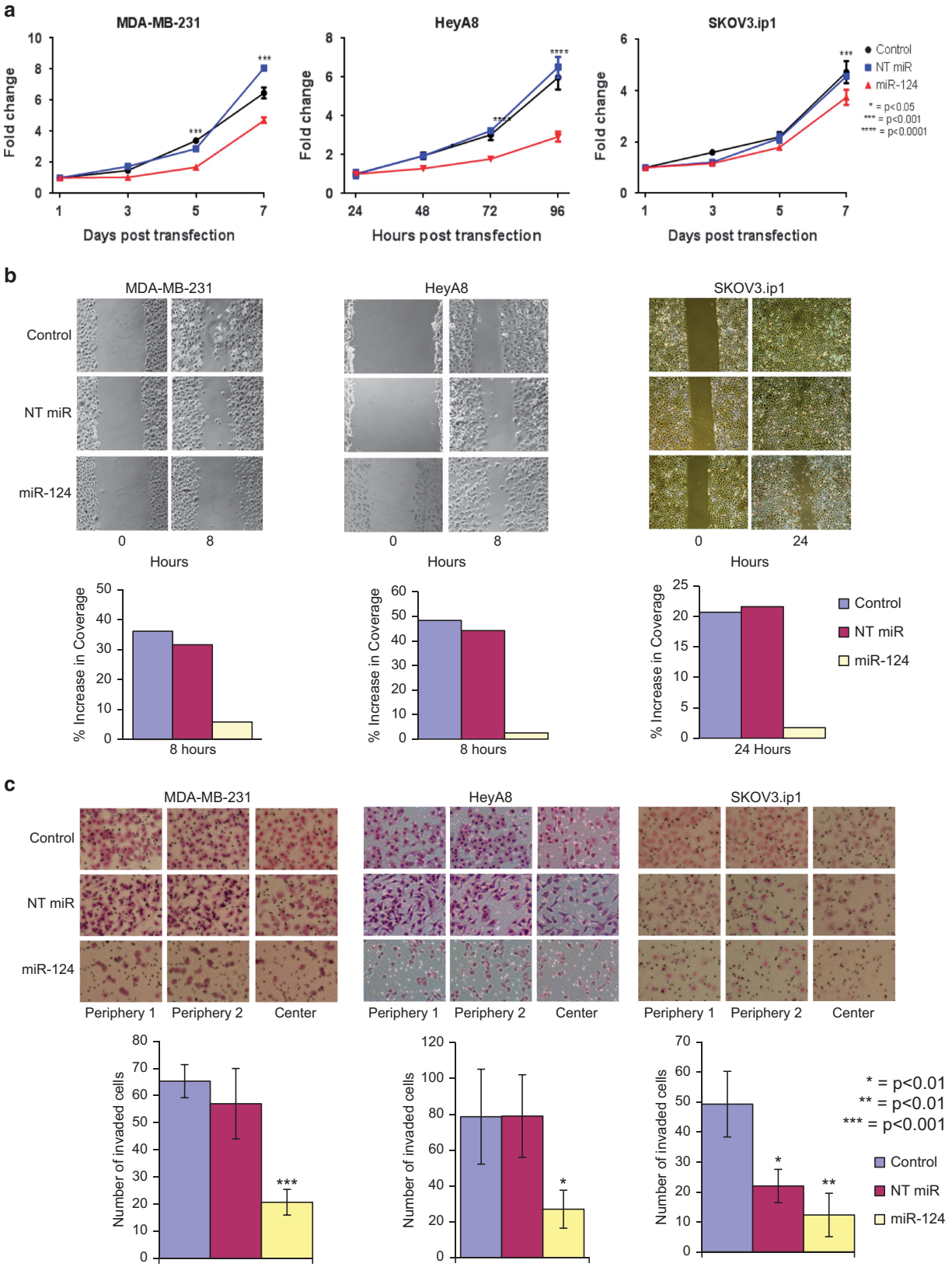

Figure 3. (Continued).

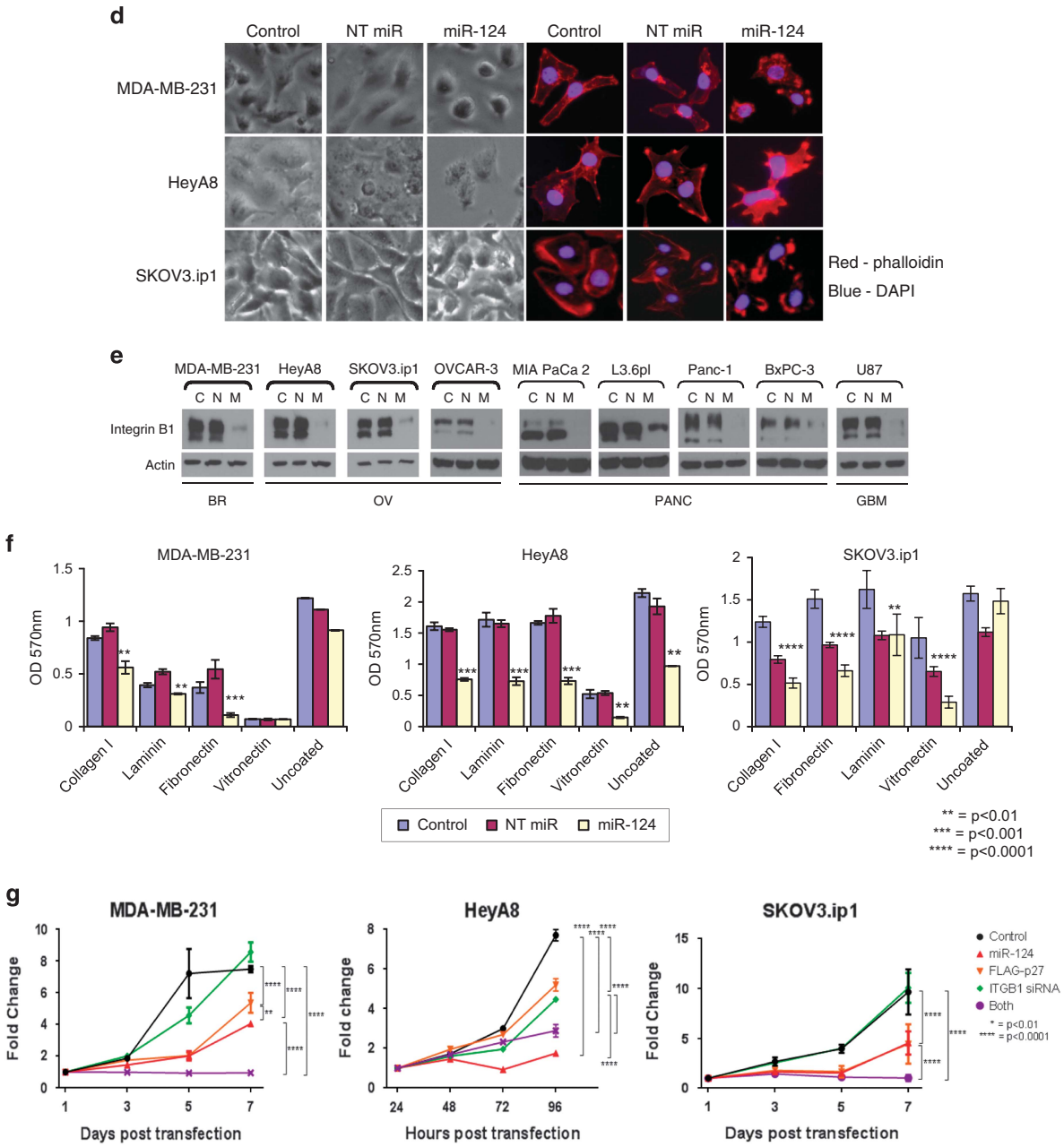

Figure 3. miR-124 functions as a tumor suppressor. (**a**) miR-124 reduces cellular proliferation. Proliferation of MDA-MB-231, HeyA8 and SKOV3.ip1 cells was analyzed at the indicated time points after transfection by staining with crystal violet and measurement of absorbance at 570 nm. Data are normalized to 24 h to indicate fold change in the cell number, and the statistical significance was determined by two-way analysis of variance. All cells were plated in triplicate. (**b**) miR-124 reduces wound healing. Cells were transfected with the indicated miRNAs and grown to form a monolayer. The monolayer was wounded with a pipette tip, and the cells were allowed to invade the wound over 8 h (for MDA-MB-231 and HeyA8) or 24 h (for SKOV3.ip1). Image analysis was carried out using the Cell Profiler image analysis software, and invasion was calculated as the increase in coverage of the central 50% of the image relative to the 0-h time point for each condition. (**c**) miR-124 expression reduces invasion. MDA-MB-231, HeyA8 and SKOV3.ip1 cells were transfected with the indicated miRNAs for 48 h before plating into Matrigel-coated invasion chambers. Invaded cells were counted using the Cell Profiler image analysis software, and statistical significance was determined using the Student's *t*-test. (**d**) miR-124 alters cellular morphology. MDA-MB-231(upper panels), HeyA8 (middle panels) and SKOV3.ip1 cells expressing miR-124 were imaged either using phase contrast or after staining with TRITC-phalloidin (red) and 4,6-diamidino-2-phenylindole (DAPI; blue). Expression of miR-124 induces rounding of the cells, with rearrangement of the actin cytoskeleton at the cell periphery. (**e**) miR-124 reduces the expression of integrin β1 in a panel of cell lines from varying tumor types, as in Figure 2a. (**f**) miR-124 reduces cellular adhesion. MDA-MB-231, HeyA8 and SKOV3.ip1 cells were transfected with miR-124, non-targeting miRNAs or treated with vehicle. After 48 h, cells were allowed to adhere to the indicated plates, and adhesion was quantified by staining with crystal violet and measuring absorbance at 570 nm. miR-124 reduces adhesion on all the substrates tested. (**g**) miR-124 requires p27 and integrin β1 for its effects on proliferation. Proliferation of MDA-MB-231, HeyA8 and SKOV3.ip1 cells was analyzed as in panel (**a**) following transfection with either miR-124 (red), integrin β1 siRNA (green), FLAG-p27 (orange) or the combination of integrin β1 siRNA and FLAG-p27 (purple).

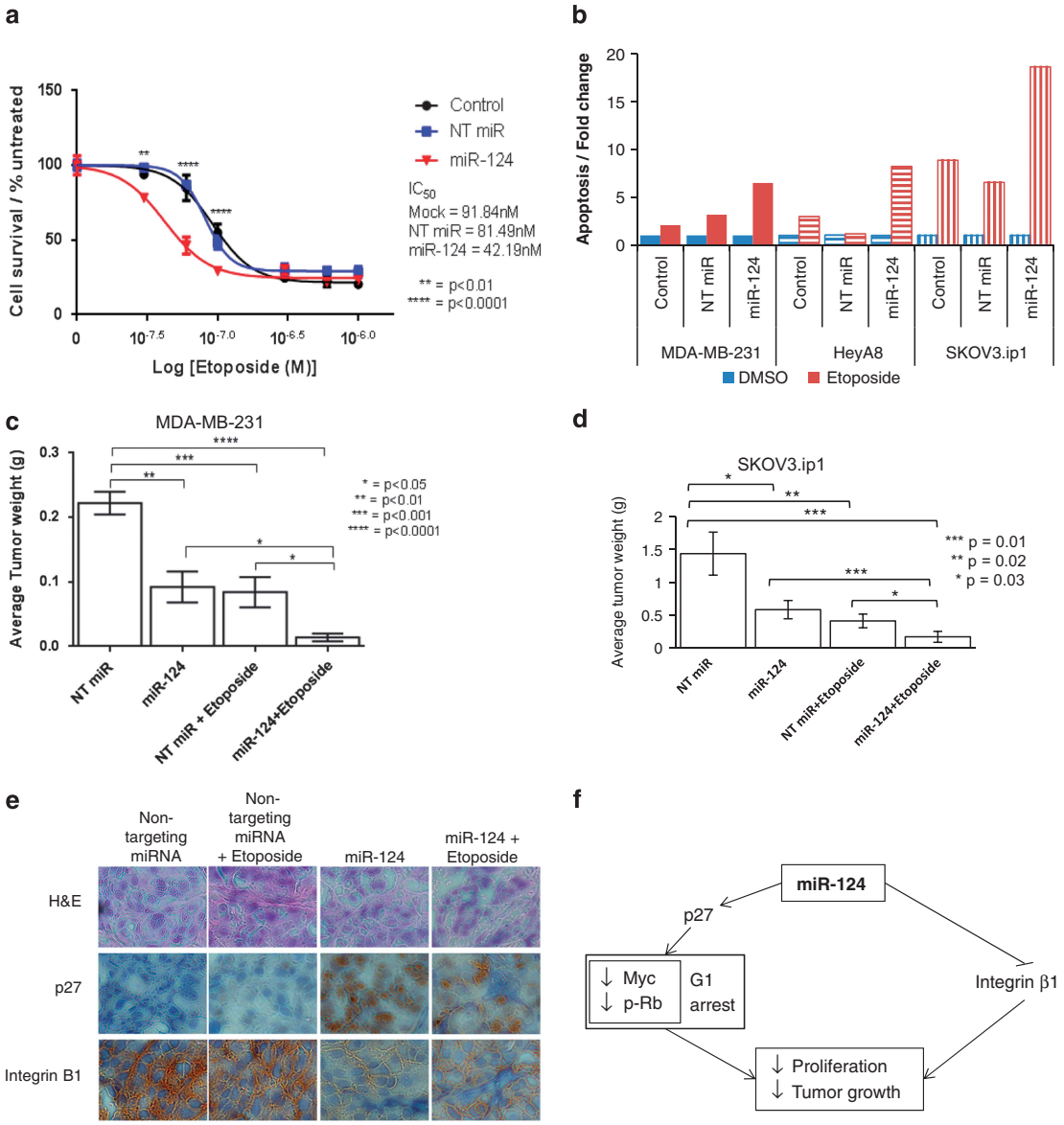

Figure 4. miR-124 functions in combination with chemotherapy. (**a**) miR-124 sensitizes cells to etoposide treatment. HeyA8 cells were transfected with the indicated miRNAs for 24 h before treatment with varying concentrations of etoposide for 72 h. Cell survival was determined by crystal violet staining and measurement of absorbance at 570 nm. Data are normalized to DMSO-treated cells. (**b**) MDA-MB-231 (solid bars) HeyA8 (horizontal stripes) and SKOV3.ip1 (vertical stripes) cells were transfected with the indicated miRNAs for 24 h before treatment with the relevant IC_{50} (red bars) or DMSO (blue bars) for 72 h. Data are normalized to DMSO treatment for each transfection and are representative of 3 independent experiments. (**c**) miR-124 reduces breast tumor growth *in vivo* and sensitizes tumor cells to etoposide. Mice were injected with MDA-MB-231 cells followed by twice weekly injection with the indicated miRNAs and once weekly injection with etoposide. Results show that either miR-124 or etoposide alone are effective in reducing tumor burden, with an additive effect of miR-124 with etoposide treatment. Statistical significance was determined using Student's *t*-test. (**d**) miR-124 reduces ovarian tumor growth *in vivo* and sensitizes tumor cells to etoposide. Mice were injected with SKOV3.ip1 cells followed by twice weekly injection with the indicated miRNAs and once weekly injection with etoposide, as detailed in panel (**c**). (**e**) miR-124 alters protein levels *in vivo*. Immunohistochemical staining of SKOV3.ip1 tumor sections shows that miR-124 reduces integrin β1 levels and increases p27 levels *in vivo*, while etoposide has no effect on protein levels. (**f**) miR-124 as a master regulator of tumor progression. miR-124 functions as a tumor suppressor by regulating both the cell cycle through induction of p27 and the response to etoposide through the downregulation of integrin β1.

reducing myc and phospho-Rb and inhibiting integrin β1 presents an exciting opportunity for the potential therapeutic use of miR-124 in combination with chemotherapy in late-stage breast and ovarian cancer patients.

MATERIALS AND METHODS

TCGA data

TCGA patient level-3 data and clinical data were downloaded from the TCGA data portal (https://tcga-data.nci.nih.gov/tcga/); GISTIC copy number data were obtained from cBioPortal (http://www.cbioportal.org/public-portal/).

Protein signature

Patient samples were grouped by myc, phospho-Rb and p27 protein levels. To assign samples to groups, the samples were scored if the protein levels were above or below a given quantile cutoff. Different quantile cutoffs were tried. Samples with myc and phospho-Rb protein expression above a given cutoff were given a score of 1 for each. Samples with p27 protein expression below a given cutoff were given a score of 1. All scores were

summed to give an aggregate score for each patient based on the expression levels of these three proteins. Patients were assigned to the protein signature group if they had a score of 2 or 3 and were excluded if their score was 1 or 0. Random quantile cutoffs were sampled from 0.3 to 0.7, and Kaplan–Meier analysis and log-rank test was run for 500 random cutoffs and the cutoffs with the lowest associated *P*-value were selected.

miRNA library screen by RPPA

The miRNA library containing 879 miRNA mimics was designed and synthesized by Dharmacon (Lafayette, CO, USA). MDA-MB-231 cells were seeded (3750 cells/well) and transfected with 50 nM miRNA. After 48 h, cells were lysed, and RPPA was carried out as previously described.[46] Further details of RPPA technology and data are available from TCGA—RPPA (http://cancergenome.nih.gov/).[47–51]

Cell titer blue assay

Changes in the cell number were determined 48 h after transfection using the cell titer blue assay (Promega, Madison, WI, USA) according to the manufacturer's instructions.

Data pretreatment

The data was normalized for plate variation.[3] For screen 1, the expression levels of proteins were normalized with respect to the mean of the expression levels of the controls (mock and non-targeting). This gives the fold change data $FP_{i,j}$ for observation i and protein j for $j = 1,\ldots,n$ where n is the number of proteins. The discrete data can then be computed as follows: For antibody j, compute the fold change s.d. $FSTD_j$ for the fold change data of the 44 controls. If $|FP_{i,j} - 1| > 2.33 \times FSTD_j$, then the expression level is 2% significantly low/high.

The data can be converted into discrete form by setting Discrete Protein expression:

$DP_{i,j} = -1$, if $|FP_{i,j} - 1| \leqslant -2.33 \times FSTD_j$;
$DP_{i,j} = 0$, if $|FP_{i,j} - 1| > -2.33 \times FSTD_j$ and $|FP_{i,j} - 1| < 2.33 \times FSTD_j$; and
$DP_{i,j} = 1$, if $|FP_{i,j} - 1| \geqslant 2.33 \times FSTD_j$.

For the second screen, the fold change of protein expression levels can be determined as above, but due to the lower number of controls, the s.d. of the controls from the first screen was used to transform the continuous fold change data into discrete data as above.

Cell culture

MDA-MB-231, HeyA8 and SKOV3.ip1 cells were maintained in RPMI with 5% (v/v) fetal bovine serum; SKBr3, OVCAR-3, BxPC-3 and L3.6pl cells were maintained in RPMI with 10% (v/v) fetal bovine serum; and MIA PaCa 2, Panc1, U87, SNB19 and LN229 cells were maintained in Dulbecco's modified Eagle's medium with 10% (v/v) fetal bovine serum. All media was also supplemented with 100 IU/ml penicillin, 100 ug/ml streptomycin and 0.25 ug/ml amphotericin B, and all cells were maintained at 37 °C with 5% CO_2. Transfections were carried out at approximately 70% confluency using 20 nM miRNA mimics (Dharmacon) and the appropriate DharmaFECT reagent (Dharmacon), according to the manufacturer's instructions.

miRNA expression analysis

Total RNA was extracted and enriched for small RNA species from the indicated cell lines using the miRVana miRNA Isolation Kit (Life Technologies, Grand Island, NY, USA). miRNA expression was analyzed using the nCounter miRNA Expression Analysis Kit (Nanostring, Seattle, WA, USA), according to the manufacturer's instructions.

SDS–PAGE (sodium dodecyl sulfate-polyacrylamide gel electrophoresis) and western blotting

Cells were transfected as described above and incubated for 48 h. Proteins were extracted in the appropriate volume of lysis buffer, and 30 µg protein was denatured in 0.2 volumes 5× SDS–PAGE loading buffer before loading onto appropriate percentage of SDS–PAGE gels. Proteins were transferred to polyvinylidene difluoride membrane and blocked for 20 min with 3% (w/v) bovine serum albumin in phosphate-buffered saline-Tween (PBS-T) at room temperature. Primary antibody incubations were carried out for 1 h at room temperature in 3% bovine serum albumin in PBS-T at the manufacturer's recommended dilution, following which membranes were washed three times for 5 min each in PBS-T. Horseradish peroxidase-conjugated secondary antibodies (Thermo Scientific, Waltham, MA, USA) were diluted 1:10 000 in 5% milk in PBS-T and incubated with membranes for 1 h at room temperature, followed by three washes for 5 min each in PBS-T. Proteins were visualized using Immobilon western chemiluminescent horseradish peroxidase substrate (Millipore, Billerica, MA, USA).

Cycloheximide chase

Cells were transfected as indicated for 24 h. Control (0-h time point) cells were lysed and prepared for western blotting as described above. The media was removed from the remaining cells and replaced with media containing either 50 ug/ml cycloheximide or 0.1% (v/v) dimethyl sulfoxide (DMSO). Cells were incubated at 37 °C and lysed at the indicated time points for analysis by western blotting.

Luciferase activity

Cells were plated into 96-well plates (5000 cells/well) and transfected with miRNAs as indicated in combination with a plasmid encoding either the GAPDH (glyceraldehyde 3-phosphate dehydrogenase) promoter or the p27 promoter upstream of the luciferase gene (Switchgear Genomics, Carlsbad, CA, USA). Twelve hours after transfection, cells were lysed, and luciferase activity determined using the Lightswitch Assay Kit (Switchgear Genomics). Activity at the p27 promoter was determined by normalizing the luciferase signal to that from the GAPDH promoter for each condition. Where indicated, the following mutations were introduced into the miR-124-binding site in the p27 promoter A*TTCCGT*CGC.

Cell cycle analysis

Cells were plated into 10-cm plates and transfected as described above. Where indicated, cells were also transfected with 50 nM control siRNA or 50 nM siRNA targeting p27 (Dharmacon). After 48 h, cells were washed, counted and resuspended in PBS (1×10^6 to 10^7 cells in 0.5 ml). Cells were added to 4.5 ml of 70% ethanol in PBS in 12×75 mm^2 centrifuge tubes for fixation and kept at −20 °C for at least 2 h. The cells were washed in 2 ml PBS and incubated at 37 °C for 15 min with 1 ml propidium iodide (0.1%(v/v) Triton X-100 in PBS, 0.2 mg/ml RNase A, 0.02 mg/ml propidium iodide). Cell cycle phase was determined by flow cytometry and analyzed with the DNA content histogram deconvolution software Cell Quest Pro (BD Biosciences, San Diego, CA, USA) by MD Anderson Flow Cytometry core.

Determination of cellular proliferation

Cells were transfected for 6 h, following which the cells were plated at 1500 cells/well in triplicate in 96-well plates. At the indicated time points, the media was removed, and adherent cells were stained with 50 µl crystal violet solution (0.5% crystal violet (w/v), 20% methanol (v/v)). After rinising to remove the excess stain, the wells were dried, and the crystals were redissolved with 100 µl 20% acetic acid (v/v). Cell density was determined by measuring the absorbance at 570 nm using a Vmax kinetic microplate reader (Molecular Devices, Sunnyvale, CA, USA). Statistical significance was determined by using two-way analysis of variance.

Wound healing

Cells were transfected in six-well plates and grown for 48 h to form a monolayer. The monolayer was wounded by scratching with a pipette tip, and the movement of cells into the wound was monitored by phase-contrast microscopy. Image analysis was carried out using Cell Profiler image analysis software (Broad Institute, Cambridge, MA, USA), and invasion was calculated as the increase in coverage of the central 50% of the image relative to the 0-h time point for each condition.

Invasion

Cells were transfected as indicated for 48 h as described above. Matrigel-coated invasion chambers (BD Biosciences) were used according to the manufacturer's instructions with media containing 5% (v/v) fetal bovine serum as a chemoattractant. After 24 h, the non-invaded cells were removed, and the invaded cells were fixed and stained using the Diff-Quick Stain Kit (IMEB Inc., San Marcos, CA, USA). Inserts were air dried and mounted onto microscopic slides using fluorescence mounting medium (Dako, Carpinteria, CA, USA). Cells were counted using Cell Profiler image analysis software.

Phalloidin staining

Cells were plated onto glass coverslips and transfected as described above. After 48 h, cells were rinsed in PBS and fixed in 4% methanol-free paraformaldehyde in PBS for 10 min at room temperature, followed by two more washes with PBS. Cells were permeabilized by incubation in 0.1% (v/v) Triton X-100 in PBS for 5 min at room temperature and washed twice in PBS. Cells were incubated in 1% (w/v) bovine serum albumin in 0.1% Triton X-100 in PBS for 20 min at room temperature followed by incubation with alexa 594-conjugated phalloidin (one unit per coverslip) diluted in blocking solution for 20 min at room temperature in the dark. After washing twice in PBS, coverslips were mounted onto microscopic slides using Vectashield mounting medium containing 4,6-diamidino-2-phenylindole.

Cellular adhesion

Cells were plated into 10-cm plates and transfected as described above. After 48 h, cells were resuspended at 1×10^6 cells/ml in non-enzymatic dissociation buffer supplemented with 1 mM each $CaCl_2$, $MgCl_2$ and $MnCl_2$. Strips (1×8) of 96-well plates precoated with the indicated extracellular matrix protein were rehydrated with 100 µl PBS for 15 min at room temperature, following which 100 µl of the relevant cell suspension was plated into the wells in triplicate. Cells were allowed to adhere for 3 h at 37 °C, after which the wells were aspirated to remove non-adherent cells. Cells were stained with crystal violet solution as previously described. Statistical significance was determined using the Student's *t*-test.

Etoposide treatment

Cells were transfected and plated as described for proliferation assays. Twenty-four hours after transfection, medium was replaced with complete medium containing etoposide in DMSO or DMSO only. After 72 h, the medium was removed, and cell survival was determined by crystal violet staining as described above.

Apoptosis detection

Cells were plated and transfected as described above. Twenty-four hours after transfection, medium was replaced with complete medium containing 100 nM etoposide (for HeyA8) or 10 µM (for MDA-MB-231 and SKOV3.ip1) in DMSO or DMSO only. After 72 h, apoptosis was assessed by the Apo-BrdU Apoptosis Detection Kit (BD Biosciences), according to the manufacturer's instructions.

In vivo

Mice were injected with MDA-MB-231 or SKOV3.ip1 cells (8×10^5 cells/mouse) and randomly separated into the indicated groups (non-targeting miRNAs, miR-124, non-targeting miRNA+etoposide and miR-124+etoposide). Mice were injected with miRNA (200 µg/kg) twice weekly, starting on day 4 after initial injection and injected with etoposide (20 mg/kg) once weekly where indicated, starting on day 9 after initial injection. Mice were killed 52 days after initial injection. Histology and immunology staining was carried out by MD Anderson Histology Core.

CONFLICT OF INTEREST

The authors declare no conflict of interest.

ACKNOWLEDGEMENTS

All the data reported are presented and available in the Supplementary Materials. The work presented here was funded by an NIH/NCI ICBP grant U54-CA112970 to JWG (Project 1 Co-PI SM, Project 2 PI-JWG, Project 4 Co-PI's PTR and GBM) and the Blanton Davis Foundation. TM is partly funded by the Odessy Fellowship (MDACC) and ZL and VS are funded by the CCBTP training grant from the CPRIT.

REFERENCES

1 Evan G. Cancer. Taking a back door to target Myc. *Science* 2012; **335**: 293–294.
2 Schmidt EV. The role of c-myc in cellular growth control. *Oncogene* 1999; **18**: 2988–2996.
3 Obaya AJ, Mateyak MK, Sedivy JM. Mysterious liaisons: the relationship between c-Myc and the cell cycle. *Oncogene* 1999; **18**: 2934–2941.
4 Miller DM, Thomas SD, Islam A, Muench D, Sedoris K. c-Myc and cancer metabolism. *Clin Cancer Res* 2012; **18**: 5546–5553.
5 Gao P, Tchernyshyov I, Chang TC, Lee YS, Kita K, Ochi T *et al.* c-Myc suppression of miR-23a/b enhances mitochondrial glutaminase expression and glutamine metabolism. *Nature* 2009; **458**: 762–765.
6 Coller HA, Grandori C, Tamayo P, Colbert T, Lander ES, Eisenman RN *et al.* Expression analysis with oligonucleotide microarrays reveals that MYC regulates genes involved in growth, cell cycle, signaling, and adhesion. *Proc Natl Acad Sci USA* 2000; **97**: 3260–3265.
7 Shiio Y, Donohoe S, Yi EC, Goodlett DR, Aebersold R, Eisenman RN. Quantitative proteomic analysis of Myc oncoprotein function. *EMBO J* 2002; **21**: 5088–5096.
8 Chandramohan V, Mineva ND, Burke B, Jeay S, Wu M, Shen J *et al.* c-Myc represses FOXO3a-mediated transcription of the gene encoding the p27(Kip1) cyclin dependent kinase inhibitor. *J Cell Biochem* 2008; **104**: 2091–2106.
9 Yang W, Shen J, Wu M, Arsura M, FitzGerald M, Suldan Z *et al.* Repression of transcription of the p27(Kip1) cyclin-dependent kinase inhibitor gene by c-Myc. *Oncogene* 2001; **20**: 1688–1702.
10 DeGregori J. The Rb network. *J Cell Sci* 2004; **117**(Pt 16): 3411–3413.
11 Polyak K, Lee MH, Erdjument-Bromage H, Koff A, Roberts JM, Tempst P *et al.* Cloning of p27Kip1, a cyclin-dependent kinase inhibitor and a potential mediator of extracellular antimitogenic signals. *Cell* 1994; **78**: 59–66.
12 Fabian MR, Sonenberg N. The mechanics of miRNA-mediated gene silencing: a look under the hood of miRISC. *Nat Struct Mol Biol* 2012; **19**: 586–593.
13 Mendell JT, Olson EN. MicroRNAs in stress signaling and human disease. *Cell* 2012; **148**: 1172–1187.
14 Lai EC. Micro RNAs are complementary to 3' UTR sequence motifs that mediate negative post-transcriptional regulation. *Nat Genet* 2002; **30**: 363–364.
15 Szymanski M, Barciszewski J. Regulation by RNA. *Int Rev Cytol* 2003; **231**: 197–258.
16 Zeng Y, Wagner EJ, Cullen BR. Both natural and designed micro RNAs can inhibit the expression of cognate mRNAs when expressed in human cells. *Mol Cell* 2002; **9**: 1327–1333.
17 Hodkinson PS, Elliott T, Wong WS, Rintoul RC, Mackinnon AC, Haslett C *et al.* ECM overrides DNA damage-induced cell cycle arrest and apoptosis in small-cell lung cancer cells through beta1 integrin-dependent activation of PI3-kinase. *Cell Death Differ* 2006; **13**: 1776–1788.
18 Hoyt DG, Rusnak JM, Mannix RJ, Modzelewski RA, Johnson CS, Lazo JS. Integrin activation suppresses etoposide-induced DNA strand breakage in cultured murine tumor-derived endothelial cells. *Cancer Res* 1996; **56**: 4146–4149.
19 Hazlehurst LA, Valkov N, Wisner L, Storey JA, Boulware D, Sullivan DM *et al.* Reduction in drug-induced DNA double-strand breaks associated with beta1 integrin-mediated adhesion correlates with drug resistance in U937 cells. *Blood* 2001; **98**: 1897–1903.
20 Zhang H, Ozaki I, Mizuta T, Matsuhashi S, Yoshimura T, Hisatomi A *et al.* Beta 1-integrin protects hepatoma cells from chemotherapy induced apoptosis via a mitogen-activated protein kinase dependent pathway. *Cancer* 2002; **95**: 896–906.
21 Luo Z, Dai Y, Zhang L, Jiang C, Li Z, Yang J *et al.* miR-18a promotes malignant progression by impairing microRNA biogenesis in nasopharyngeal carcinoma. *Carcinogenesis* 2013; **34**: 415–425.
22 Mouw JK, Yui Y, Damiano L, Bainer RO, Lakins JN, Acerbi I *et al.* Tissue mechanics modulate microRNA-dependent PTEN expression to regulate malignant progression. *Nat Med* 2014; **20**: 360–367.
23 Nam EJ, Yoon H, Kim SW, Kim H, Kim YT, Kim JH *et al.* MicroRNA expression profiles in serous ovarian carcinoma. *Clin Cancer Res* 2008; **14**: 2690–2695.
24 Xu XL, Jiang YH, Feng JG, Su D, Chen PC, Mao WM. MicroRNA-17, microRNA-18a, and microRNA-19a are prognostic indicators in esophageal squamous cell carcinoma. *Ann Thorac Surg* 2014; **97**: 1037–1045.
25 Toyoshima M, Howie HL, Imakura M, Walsh RM, Annis JE, Chang AN *et al.* Functional genomics identifies therapeutic targets for MYC-driven cancer. *Proc Natl Acad Sci USA* 2012; **109**: 9545–9550.
26 Janowski BA, Younger ST, Hardy DB, Ram R, Huffman KE, Corey DR. Activating gene expression in mammalian cells with promoter-targeted duplex RNAs. *Nat Chem Biol* 2007; **3**: 166–173.
27 Li LC, Okino ST, Zhao H, Pookot D, Place RF, Urakami S *et al.* Small dsRNAs induce transcriptional activation in human cells. *Proc Natl Acad Sci USA* 2006; **103**: 17337–17342.
28 Place RF, Li LC, Pookot D, Noonan EJ, Dahiya R. MicroRNA-373 induces expression of genes with complementary promoter sequences. *Proc Natl Acad Sci USA* 2008; **105**: 1608–1613.
29 Jopling CL, Yi M, Lancaster AM, Lemon SM, Sarnow P. Modulation of hepatitis C virus RNA abundance by a liver-specific MicroRNA. *Science* 2005; **309**: 1577–1581.
30 Cao X, Pfaff SL, Gage FH. A functional study of miR-124 in the developing neural tube. *Genes Dev* 2007; **21**: 531–536.
31 Hunt S, Jones AV, Hinsley EE, Whawell SA, Lambert DW. MicroRNA-124 suppresses oral squamous cell carcinoma motility by targeting ITGB1. *FEBS Lett* 2011; **585**: 187–192.

32 Zhang J, Lu Y, Yue X, Li H, Luo X, Wang Y *et al.* MiR-124 suppresses growth of human colorectal cancer by inhibiting STAT3. *PLoS One* 2013; **8**: e70300.
33 Shi XB, Xue L, Ma AH, Tepper CG, Gandour-Edwards R, Kung HJ *et al.* Tumor suppressive miR-124 targets androgen receptor and inhibits proliferation of prostate cancer cells. *Oncogene* 2013; **32**: 4130–4138.
34 Liang YJ, Wang QY, Zhou CX, Yin QQ, He M, Yu XT *et al.* MiR-124 targets Slug to regulate epithelial-mesenchymal transition and metastasis of breast cancer. *Carcinogenesis* 2013; **34**: 713–722.
35 Lang Q, Ling C. MiR-124 suppresses cell proliferation in hepatocellular carcinoma by targeting PIK3CA. *Biochem Biophys Res Commun* 2012; **426**: 247–252.
36 Xia H, Cheung WK, Ng SS, Jiang X, Jiang S, Sze J *et al.* Loss of brain-enriched miR-124 microRNA enhances stem-like traits and invasiveness of glioma cells. *J Biol Chem* 2012; **287**: 9962–9971.
37 Zheng F, Liao YJ, Cai MY, Liu YH, Liu TH, Chen SP *et al.* The putative tumour suppressor microRNA-124 modulates hepatocellular carcinoma cell aggressiveness by repressing ROCK2 and EZH2. *Gut* 2012; **61**: 278–289.
38 Xia J, Wu Z, Yu C, He W, Zheng H, He Y *et al.* miR-124 inhibits cell proliferation in gastric cancer through down-regulation of SPHK1. *J Pathol* 2012; **227**: 470–480.
39 Wei J, Wang F, Kong LY, Xu S, Doucette T, Ferguson SD *et al.* miR-124 inhibits STAT3 signaling to enhance T cell-mediated immune clearance of glioma. *Cancer Res* 2013; **73**: 3913–3926.
40 Li CX, Parker A, Menocal E, Xiang S, Borodyansky L, Fruehauf JH. Delivery of RNA interference. *Cell Cycle* 2006; **5**: 2103–2109.
41 Akbani R, Ng PK, Werner HM, Shahmoradgoli M, Zhang F, Ju Z *et al.* A pan-cancer proteomic perspective on The Cancer Genome Atlas. *Nat Commun* 2014; **5**: 3887.
42 Kang S, Zhao Y, Hu K, Xu C, Wang L, Liu J *et al.* miR-124 exhibits antiproliferative and antiaggressive effects on prostate cancer cells through PACE4 pathway. *Prostate* 2014; **74**: 1095–1106.
43 Li Y, Zhang Z, Liu X, Huang T, He W, Shen Y *et al.* miR-124 functions as a tumor suppressor in the endometrial carcinoma cell line HEC-1B partly by suppressing STAT3. *Mol Cell Biochem* 2013; **388**: 219–231.
44 Lu Y, Yue X, Cui Y, Zhang J, Wang K. MicroRNA-124 suppresses growth of human hepatocellular carcinoma by targeting STAT3. *Biochem Biophys Res Commun* 2013; **441**: 873–879.
45 Pecot CV, Rupaimoole R, Yang D, Akbani R, Ivan C, Lu C *et al.* Tumour angiogenesis regulation by the miR-200 family. *Nat Commun* 2013; **4**: 2427.
46 Lu Y, Muller M, Smith D, Dutta B, Komurov K, Iadevaia S *et al.* Kinome siRNA-phosphoproteomic screen identifies networks regulating AKT signaling. *Oncogene* 2011; **30**: 4567–4577.
47 Cancer Genome Atlas N, Comprehensive molecular portraits of human breast tumours. *Nature* 2012; **490**: 61–70.
48 Cancer Genome Atlas N, Comprehensive molecular characterization of human colon and rectal cancer. *Nature* 2012; **487**: 330–337.
49 Cancer Genome Atlas Research N, Comprehensive genomic characterization defines human glioblastoma genes and core pathways. *Nature* 2008; **455**: 1061–1068.
50 Cancer Genome Atlas Research N, Integrated genomic analyses of ovarian carcinoma. *Nature* 2011; **474**: 609–615.
51 Cancer Genome Atlas Research N, Comprehensive genomic characterization of squamous cell lung cancers. *Nature* 2012; **489**: 519–525.

Supplementary Information accompanies this paper on the Oncogene website (http://www.nature.com/onc)